AIP | Applied Physics Letters

Comparison of majority carrier charge transfer velocities at Si/polymer and Si/metal photovoltaic heterojunctions

Michelle J. Price, Justin M. Foley, Robert A. May, and Stephen Maldonado

Citation: Applied Physics Letters **97**, 083503 (2010); doi: 10.1063/1.3480599
View online: http://dx.doi.org/10.1063/1.3480599
View Table of Contents: http://scitation.aip.org/content/aip/journal/apl/97/8?ver=pdfcov
Published by the AIP Publishing

Comparison of majority carrier charge transfer velocities at Si/polymer and Si/metal photovoltaic heterojunctions

Michelle J. Price,[1] Justin M. Foley,[1] Robert A. May,[2] and Stephen Maldonado[1,3,a)]
[1]*Applied Physics Program, University of Michigan, 450 Church Street, Ann Arbor, Michigan 48109-1040, USA*
[2]*Department of Chemistry and Biochemistry, University of Texas at Austin, 1 University Station A5300, Austin, Texas 78712-0165, USA*
[3]*Department of Chemistry, University of Michigan, 930 N University, Ann Arbor, Michigan 48109-1055, USA*

(Received 22 May 2010; accepted 25 July 2010; published online 23 August 2010)

Two sets of silicon (Si) heterojunctions with either Au or PEDOT:PSS contacts have been prepared to compare interfacial majority carrier charge transfer processes at Si/metal and Si/polymer heterojunctions. Current-voltage (*J-V*) responses at a range of temperatures, wavelength-dependent internal quantum yields, and steady-state *J-V* responses under illumination for these devices are reported. The cumulative data suggest that the velocity of majority carrier charge transfer, v_n, is several orders of magnitude smaller at n-Si/PEDOT:PSS contacts than at n-Si/Au junctions, resulting in superior photoresponse characteristics for these inorganic/organic heterojunctions. © *2010 American Institute of Physics*. [doi:10.1063/1.3480599]

There are three types of inorganic/organic semiconductor heterojunctions for light-harvesting: (i) an organic chromophore is the primary light absorber and selectively injects photogenerated carriers into an inorganic semiconductor for transport to an electrical contact,[1] (ii) both inorganic and organic components absorb light and transport photogenerated carriers,[2] and (iii) an inorganic semiconductor is the primary light absorber and the medium for photogenerated carrier transport while an organic material is a transparent, carrier-selective contact.[3,4] Heterojunctions of the third type are attractive because they utilize the broadband absorption and good charge transport properties of inorganic semiconductors and are less prone to photodegradation than systems with organic chromophores. A detailed understanding of charge-transfer processes at these inorganic/organic heterojunctions is necessary for further design and development. In this letter, the intrinsic light energy conversion properties of Si/polymer and Si/metal heterojunctions are contrasted. Poly(3,4-ethylenedioxythiophene) poly(styrenesulfonic acid) (PEDOT:PSS), a commercial conductive polymer blend with a work function (5.1 eV) comparable to that of Au,[5] is used as the transparent organic contacting material.

The impedance characteristics of n-Si/Au and n-Si/PEDOT:PSS contacts were collected and are detailed in Ref. 27. The agreement of the C^{-2}-*V* responses between 0.65 and 65 kHz and the linearity of the Bode slopes validated using a simple parallel *RC* network to model both device types. The interfacial equilibrium barrier heights (Φ_b) from these data were 0.80 ± 0.01 and 0.89 ± 0.02 V for n-Si/Au and n-Si/PEDOT:PSS contacts, respectively. Both n-Si/Au and n-Si/PEDOT:PSS contacts demonstrated strongly rectifying *J-V* responses while both p-Si/Au and p-Si/PEDOT:PSS contacts yielded "Ohmic" *J-V* responses at room temperature (Ref. 27). For rectifying contacts where thermal activation of majority carriers over an interfacial potential energy barrier is rate-limiting, J_0 contains information on the majority carrier charge-transfer rate,[6]

$$J(V) = J_0(e^{qV/k_BT} - 1) = qN_{CB}v_n e^{-q\Phi_b/k_BT}(e^{qV/k_BT} - 1), \quad (1)$$

where v_n is the majority-carrier (electron) charge transfer velocity (cm s^{-1}) across the front interface, q is the electron charge, N_{CB} is the effective density of states in the conduction band, T is temperature, and k_B is Boltzmann's constant.[6] Equation (1) is the general form of the thermionic emission model routinely applied to Schottky heterojunctions.[6] The pre-exponential term in Eq. (1) can be determined from an analysis of J_0 at several temperatures.[7] A representative set of temperature-dependent *J-V* responses for n-Si/PEDOT:PSS contacts is shown in Fig. 1(a). For these devices, current densities at low forward bias were temperature dependent in accord with thermionic emission, rather than space-charge limited conduction[8] in PEDOT:PSS or the ionization of surface traps.[9] Values of J_0 were obtained by linear extrapolation of $J(V)$ to $V=0$ V. The temperature dependence of J_0 for n-Si/PEDOT:PSS contacts, along with corresponding data for a n-Si/Au heterojunction, are shown in Fig. 1(b). The strong linearity for both Si/Au and Si/PEDOT:PSS is consistent with the premise that the intercepts report on the values of v_n. The data for the n-Si/Au heterojunction corresponded to $v_{n,Au} = 1.7 \times 10^7$ cm s^{-1}, in accord with the known majority carrier charge-transfer velocity at Si/metal

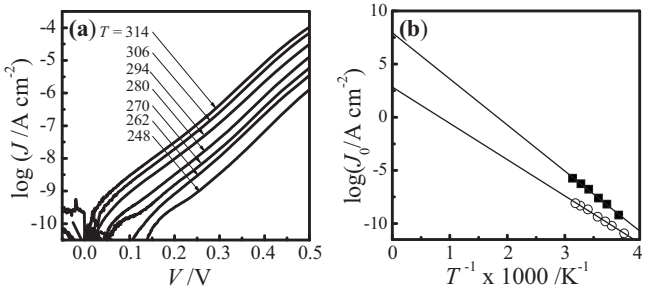

FIG. 1. (a) Forward bias *J-V* response for a n-Si/PEDOT:PSS device measured at several temperatures (K). (b) Temperature dependence of J_0 for (■) n-Si/Au and (○) n-Si/PEDOT:PSS contacts.

a)Author to whom correspondence should be addressed. Tel.: 734-647-4750. Electronic mail: smald@umich.edu.

contacts.[6] In contrast, $v_{n,PEDOT:PSS}=1.3\times10^{2}$ cm s^{-1}. Replicate measurements consistently gave values of $v_{n,PEDOT:PSS}$ several orders of magnitude smaller than $v_{n,Au}$, ranging from 0.88 to 660 cm s^{-1} (Ref. 27).

A separate comparison of v_n values was obtained from photoresponses. The internal quantum yield $\eta(\lambda)$ for an illuminated semiconductor heterojunction is sensitive to both minority and majority carrier processes and is given by Eq. (2),[10]

$$\eta(\lambda)=1-\frac{e^{-\alpha(\lambda)W}}{1+\alpha(\lambda)L_p}-\frac{1}{\left[1+\frac{qE_0}{\alpha(\lambda)k_BT}\right]\left(1+\frac{\mu_nE_0}{v_n}\right)}, \quad (2)$$

where L_p is the minority carrier diffusion length, α is the absorptivity, W is the depletion width, E_0 is the electric field at the interface, and μ_n is the electron mobility. The middle term on the right side describes minority carrier recombination losses within the bulk.[11] The last term on the right side of Eq. (2) is an exact solution of the carrier transport equation which accounts for the competition between deleterious majority carrier charge transfer across the front contact and collection at the back contact [Fig. 2(a)].[10] This loss mechanism can be significant for carriers photogenerated near the front contact by strongly absorbed (short-wavelength) light when v_n is large.[10] Figure 2(b) shows the predicted internal quantum yield from Eq. (2) as a function of wavelength for crystalline Si heterojunctions with $N_D=6\times10^{12}$ cm^{-3}, $L_p=0.025$ cm, $\mu_n=1500$ cm^2 v^{-1} s^{-1}, and a range of v_n values between 10^4 and 10^8 cm s^{-1}. Only values of $v_n\leq10^4$ cm s^{-1} result in unit quantum yields at short wavelengths. Figure 2(c) shows the measured wavelength-dependent internal quantum yield data for a representative n-Si/Au heterojunction, fit by $v_{n,Au}=10^7$ cm s^{-1}.[12] Figure 2(d) shows the corresponding data for a representative n-Si/PEDOT:PSS heterojunction, fit by values of $v_{n,PEDOT:PSS}\leq10^4$ cm s^{-1}. Figure 2(e) shows data for a n-Si/PEDOT:PSS device prepared using CH_3-terminated Si(111) substrates,[13] also fit by $v_{n,PEDOT:PSS}\leq10^4$ cm s^{-1}.

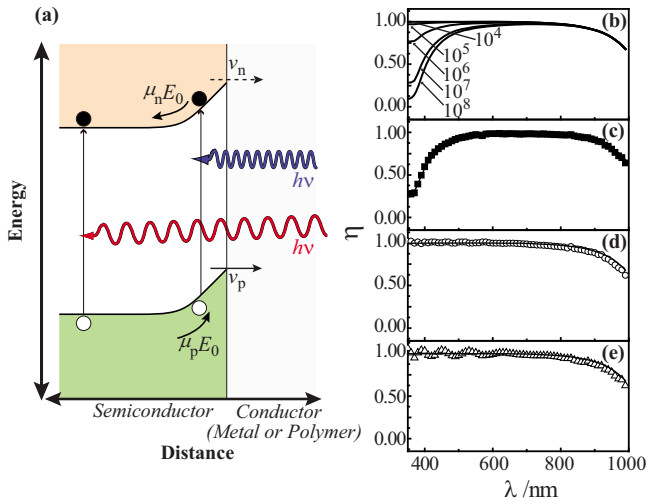

FIG. 2. (Color online) (a) Band bending diagram for a semiconductor heterojunction illuminated by short- and long-wavelength light. Solid and dashed arrows indicate favorable and deleterious processes for photogenerated carrier collection, respectively. (b) Calculated wavelength-dependent internal quantum yields for Si heterojunctions with $\mu_n=1500$ cm^2 V^{-1} s^{-1}, $L_p=.025$ cm, and several values of v_n(cm s^{-1}). (c) Measured wavelength-dependent internal quantum yield for a representative n-Si/Au contact. The solid line is a fit with $v_n=10^7$ cm s^{-1}. (d) Measured wavelength-dependent internal quantum yield for a representative n-Si/PEDOT:PSS device. The solid line is a fit with $v_n=10^4$ cm s^{-1}. (e) Measured wavelength-dependent internal quantum yield for a representative n-Si/PEDOT:PSS device made with CH_3-terminated n-Si(111). The solid line is a fit with $v_n=10^4$ cm s^{-1}.

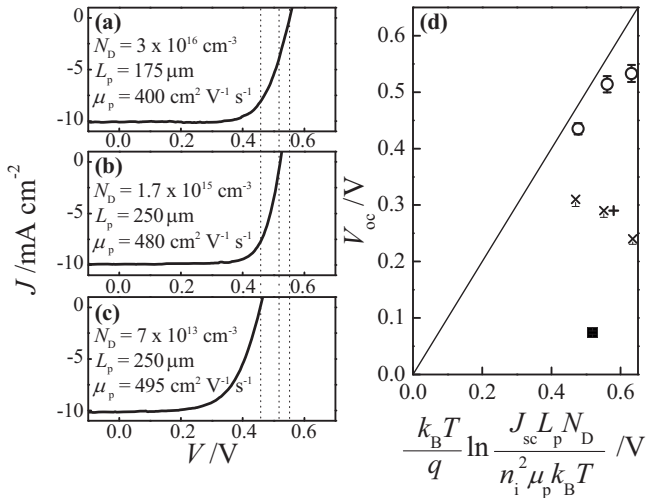

FIG. 3. Representative steady-state *J-V* responses under white-light illumination for n-Si/PEDOT:PSS heterojunctions with various bulk optoelectronic properties. V_{oc} values are indicated by dashed lines. (d) Measured V_{oc} values from Figs. 3(a)–3(c) as a function of the maximum expected V_{oc} values from Eq. (3). Responses for n-Si/Au devices from (×) (Ref. 22) and (+) (Ref. 21) and (■) a control sample. The solid line represents the maximum attainable V_{oc} values set by bulk recombination.

Steady-state *J-V* responses under white-light illumination were also assessed for a series of n-Si/PEDOT:PSS heterojunctions. In Figs. 3(a)–3(c), the *x*-axis intercept is the open-circuit photovoltage, V_{oc}, at an illumination intensity that corresponds to a short-circuit current density, J_{sc}, of 10 mA cm^{-2}. For a semiconductor heterojunction under a constant photon flux, V_{oc} is proportional to $\ln(J_{sc}/J_0)$.[6] Factors that decrease J_0 naturally augment the photovoltage. However, the lower limit for J_0 is finite and set by the carrier recombination rate in the bulk determined by the bulk optoelectronic properties of Si.[6] The largest attainable value of V_{oc} under low-level injection conditions[14] is thus

$$V_{oc}=\frac{k_BT}{q}\ln\left(\frac{J_{sc}L_pN_D}{n_i^2\mu_pk_BT}\right), \quad (3)$$

where μ_p is the mobility of holes, N_D is the dopant density, and n_i is the intrinsic carrier concentration in Si. The values of V_{oc} from Figs. 3(a)–3(c) and Table S4 (Ref. 27) are presented in Fig. 3(d) as a function of the maximum attainable V_{oc} predicted by Eq. (3) from the Si bulk properties for each device. Illumination data from past reports of n-Si/Au heterojunctions are also shown for comparison. For devices limited purely by thermionic emission, Eq. (1) does not predict any strong dependence of the photoresponses with L_p, μ_p, or N_D. In contrast, the values of V_{oc} for n-Si/PEDOT:PSS devices were sensitive to these optoelectronic properties and approached, but did not reach, the limit set by bulk recombination. These data suggest V_{oc} values were not limited entirely by either thermionic emission or bulk-recombination. The black solid square in Fig. 3(d) corresponds to the value of V_{oc} recorded for a modified n-Si/Au heterojunction prepared by exposing the Si substrate to the supernatant of the PEDOT:PSS casting solution, then heating and handling the substrate in an analogous fashion to the Si substrates contacted with PEDOT:PSS, and finally contacting

with Au. These devices yielded significantly lower V_{oc} values than corresponding n-Si/PEDOT:PSS contacts.

Figures 1–3 indicate v_n is intrinsically slower by several orders of magnitude at n-Si/PEDOT:PSS than at n-Si/Au contacts. Although differences in bulk charge-carrier conduction can negatively impact performance and contribute to long-term degradation mechanisms,[8,15] a recent report on PEDOT:PSS/Si nanowire composites illustrates the utility of these heterojunctions as solar cells.[16] Inorganic semiconductor/conducting polymer heterojunctions are often analyzed using the formalism developed for Schottky solid-state devices.[3,7,17] Lonergan and co-workers previously reported anomalously small J_0 values for InP/polypyrrole contacts, identifying an attenuation factor that affected the Richardson constant (A^{**}) for InP/metal contacts.[9] The "v_n" formalism used here describes analogous observations but also highlights a direct connection to microscopic theories of charge transfer. The parameter v_n describes the product of the standard rate constant for majority carrier charge transfer, $k_{et}(\mathrm{cm}^4\ \mathrm{s}^{-1})$, and the effective density of acceptor states in the contacting material, $N_A(\mathrm{cm}^{-3})$. A diminution in k_{et}, N_A, or both results in smaller values of v_n. In Si/metal contacts where k_{et} and N_A are large, fast charge transfer rates are masked by the thermal velocity of carriers within Si ($v_n \sim 10^7$ cm s^{-1}).[12] This value of v_n is implicit when the pre-exponential term in Eq. (1) includes A^{**}.[6]

Multiple factors may contribute to the smaller value of v_n observed in n-Si/PEDOT:PSS versus n-Si/Au heterojunctions. Semiclassical models for microscopic heterogeneous charge transfer have been used to interpret k_{et} for semiconductor/liquid heterojunctions.[18] The difficulties in determining reorganization energies in polymers,[19] in addition to the influence of grain boundaries, complicate this type of analysis for the inorganic/organic heterojunctions shown here. Nevertheless, both the presented data and existing literature on metal-insulator-semiconductor (MIS) heterojunctions argue against the possibility that k_{et} is decreased at these n-Si/PEDOT:PSS contacts solely because of an interfacial oxide. For n-Si MIS devices based on native, chemical, or evaporated surface oxides, small values of V_{oc} which do not approach the limit imposed by bulk-recombination processes are observed, in contrast to the data shown here.[20] Although sputtered oxides[20] and photoelectrochemical anodization[21] have been used to produce n-type MIS devices with good photoresponses, the conditions employed herein should not lead to chemically equivalent surface oxides. The small V_{oc} values for the control n-Si/Au devices illustrated that an inadvertent surface oxide from processing is not the defining feature for good photoresponses. Additional control n-Si/PEDOT:PSS devices made with CH_3-terminated Si(111) substrates exhibited internal quantum efficiencies consistent with $v_{n,\mathrm{PEDOT:PSS}} \ll 10^7$ cm s^{-1} [Fig. 2(e)]. Since CH_3-terminated Si(111) surfaces are strongly resistant to chemical oxidation when processed in ambient conditions and a CH_3-monolayer does not represent an appreciable tunneling barrier for electron transfer at room temperature,[13] an equivalent surface oxide that favorably affects the photoresponses of these n-Si/PEDOT:PSS heterojunctions is also unlikely.

The effective density of states at the Fermi level for Au and PEDOT:PSS are different ($\sim 10^{22}$ cm^{-3} and $\leq 10^{18}$ cm^{-3}, respectively).[6,23,24] Although the chemical composition of PEDOT determines N_A, the specific blend morphology of PEDOT:PSS films may also lower v_n by decreasing the electronic coupling between PEDOT and Si. In cast PEDOT:PSS films, the PSS component forms thin encapsulating shells around the core conducting PEDOT colloids, favoring hole transfer over electron transfer.[25] Transparent conducting polymer contacts with this feature may therefore be useful as contacts to a variety of inorganic semiconductors. A recent report that details the excellent photoresponses of amorphous-Si/PEDOT:PSS heterojunctions is consistent with this premise.[26]

In summary, the collected data cumulatively demonstrated v_n at Si heterojunctions was substantially slower when a conducting polymer was used instead of a metal contact. This work highlights the advantages of this feature for photovoltaic applications.

[1] M. Gratzel, J. Photochem. Photobiol., A **164**, 3 (2004).
[2] W. J. E. Beek, M. M. Wienk, M. Kemerink, X. N. Yang, and R. A. J. Janssen, J. Phys. Chem. B **109**, 9505 (2005).
[3] M. J. Sailor, F. L. Klavetter, R. H. Grubbs, and N. S. Lewis, Nature (London) **346**, 155 (1990).
[4] W. N. Wang and E. A. Schiff, Appl. Phys. Lett. **91**, 133504 (2007).
[5] S. Smith and S. R. Forrest, Appl. Phys. Lett. **84**, 5019 (2004).
[6] S. M. N. Sze and K. Kwok, *Physics of Semiconductor Devices*, 3rd ed. (Wiley, New York, 2007).
[7] C. Daniels-Hafer, M. Jang, S. W. Boettcher, R. G. Danner, and M. C. Lonergan, J. Phys. Chem. B **106**, 1622 (2002).
[8] L. M. Andersson, F. L. Zhang, and O. Inganas, Appl. Phys. Lett. **91**, 071108 (2007).
[9] A. Carbone, P. Mazzetti, and F. Rossi, Appl. Phys. Lett. **95**, 233303 (2009).
[10] J. Reichman, Appl. Phys. Lett. **38**, 251 (1981).
[11] W. W. Gärtner, Phys. Rev. **116**, 84 (1959).
[12] C. Jacoboni, C. Canali, G. Ottaviani, and A. A. Quaranta, Solid-State Electron. **20**, 77 (1977).
[13] S. Maldonado and N. S. Lewis, J. Electrochem. Soc. **156**, H123 (2009).
[14] J. G. Fossum, IEEE Trans. Electron Devices **24**, 322 (1977).
[15] C. Renaud and T. P. Nguyen, J. Appl. Phys. **106**, 053707 (2009).
[16] S. C. Shiu, J. J. Chao, S. C. Hung, C. L. Yeh, and C. F. Lin, Chem. Mater. **22**, 3108 (2010).
[17] D. P. Halliday, J. W. Gray, P. N. Adams, and A. P. Monkman, Synth. Met. **102**, 877 (1999).
[18] H. Gerischer, *Advances in Electrochemistry and Electrical Engineering* (Wiley, New York, 2004), Vol. 4, pp. 142–178.
[19] G. R. Hutchison, M. A. Ratner, and T. J. Marks, J. Am. Chem. Soc. **127**, 16866 (2005).
[20] D. L. Pulfrey, IEEE Trans. Electron Devices **25**, 1308 (1978).
[21] A. Kumar, M. D. Rosenblum, D. L. Gilmore, B. J. Tufts, M. L. Rosenbluth, and N. S. Lewis, Appl. Phys. Lett. **56**, 1919 (1990).
[22] S. Maldonado, D. Knapp, and N. S. Lewis, J. Am. Chem. Soc. **130**, 3300 (2008).
[23] E. G. Kim and J. L. Bredas, J. Am. Chem. Soc. **130**, 16880 (2008).
[24] The effective conduction band density of states can be estimated by $N_c = 2(2\pi m_e k_B T/h^2)^{3/2}$, where m_e is the effective electron mass.
[25] J. Hwang, F. Amy, and A. Kahn, Org. Electron. **7**, 387 (2006).
[26] E. L. Williams, G. E. Jabbour, Q. Wang, S. E. Shaheen, D. S. Ginley, and E. A. Schiff, Appl. Phys. Lett. **87**, 223504 (2005).
[27] See supplementary material at http://dx.doi.org/10.1063/1.3480599 for a full description of the materials, device preparation, experimental methods, impedance measurements, and optical corrections used to determine internal quantum yields.